Molecular Simulation, 1992, Vol. 8, pp. 361–387
Reprints available directly from the publisher
Photocopying permitted by license only

MOLECULAR DYNAMICS SIMULATIONS IN HETEROGENEOUS DIELECTRICA AND DEBYE–HÜCKEL MEDIA – APPLICATION TO THE PROTEIN BOVINE PANCREATIC TRYPSIN INHIBITOR

C. NIEDERMEIER*† and K. SCHULTEN‡

Department of Physics and Beckman Institute, University of Illinois at Urbana-Champaign, 405 N. Mathews Avenue, Urbana, IL 61801 U.S.A.

(*Received August 1980, accepted September 1990*)

1 INTRODUCTION

Solvent interactions, especially solvent-mediated dielectric screening and Debye–Hückel screening, are thought to be essential determinants of the structure and function of proteins and nucleic acids. These interactions guide the polypeptide chain towards a protein's native conformation [2, 3, 4], stabilize the B structure of DNA, govern transitions to its A form [5] and play an important role in substrate binding and enzymatic activity [6, 7, 8]. The proper description of solvent-mediated electrostatic interactions of biopolymers have received increased attention and methods have been developed to determine the electrostatic potential around biopolymers. Some of the efforts have presented water external to biopolymers by discrete descriptions either involving molecular dynamics models of water [9, 10, 11] or its representation by Langevin dipoles [12]. Other efforts have described water by a continuum model [13, 7, 14, 15].

Continuum models of water certainly lack the degree of realism of discrete models. However, they appear to be unavoidable to account for the dielectric properties of the bulk water. The necessity for continuum models derives from the long-range character of Coulomb forces which induce solvent effects. The long-range character implies that a very large number of water molecules contained in a volume with a diameter of several Debye lengths need to be modelled. For physiological solvents with a Debye length of about 8 Å this implies typically several thousand atoms to be added to a molecular dynamics simulation. The most promising avenue for a description of solvent effects should be furnished by mixed models which involve discrete water near the solute and a continuum at larger distances which accounts for the bulk water. In

*Currently at Gesellschaft für Strahlen- und Umweltforschung, Ingolstädter Landstraße 1, D-8042 Neuherberg, FRG.

†Work completed towards the requirements of the Diplom degree for C. N. at Technische Universität München, FRG [1].

‡To whom correspondence should be addressed.

this paper we address the issue relevant both for continuum and for mixed discrete-continuum solvent models, namely how a continuum representation of a solvent can be linked to a molecular dynamics description of the discrete solute or a discrete solute-water system. We consider as a solute the protein bovine pancreatic trypsin inhibitor (BPTI) which has been the subject of many prototypical molecular dynamics simulations [16, 17, 18, 19].

Most earlier investigations have considered the influence of solvents on the energetics of biopolymers, i.e., they essentially addressed equilibrium properties like free energies [20, 6, 21, 22] or pK-values [23]. In this paper we want to address the issue how a solvent influences structure and dynamics of a protein, the prediction of protein folding to the native structure constituting the ultimate goal.

At the present early stage of investigations of solvent effects on biopolymer dynamics one needs to develop proper frameworks in which the forces acting on biopolymers due to external solvents can be determined. The present paper focusses mainly on this methodological issue; the authors consider the results on solvent effects on structure and dynamics of BPTI, obtained by applying the suggested algorithms, only of secondary importance.

The main concept which underlies the link between solvent and internal dynamics of a biopolymer is the reaction field. One can define the reaction field as the field which includes all forces due to the presence of the solvent. The reaction field can be determined readily in case that solvent effects can be formally attributed to image charges [24, 25]. However, also in more general situations, the reaction field can be defined in ways which are both numerically tractable and physically transparent. The simplest algorithm determines first the potentials for a biopolymer in the presence and in the absence of the solvent, then takes the difference of these potentials, derives the respective forces and adds these forces to a conventional molecular dynamics calculation. The potential can be evaluated by solving the Poisson–Boltzmann equation numerically. Such avenue requires very efficient algorithms for the solution of this partial differential equation since the solutions need to be furnished repeatedly during a molecular dynamics simulation. However, due to the slow dielectric relaxation time and due to the relatively low mobilities of ions in the solvent which mediate Debye–Hückel screening, one needs to update the reaction field only on time scales long compared to integration time steps.

Rather than being only accessible through evaluating potentials with and without solvents, the reaction force field can also be evaluated directly and, thereby, more rapidly and accurately. This approach is well-known in the theory of electrodynamic media [26]. The related potential is the solution of a Poisson–Boltzmann equation with a charge distribution that involves a surface charge density at dielectric discontinuities and a volume charge density accounting for Debye–Hückel screening. Both for a direct and an indirect evaluation of the reaction field, the problem arises to state values of the potential on the boundary of the volume in which numerical integrations are carried out. Since the boundary is not at an infinite distance from the solute, i.e., where the potentials can be assumed to vanish, approximations need to be envoked. Beside solvent-mediated electrostatics, the dynamics of biopolymers can also be influenced by neutralization of surface charges, either through binding of ions or through protonation/deprotonation processes. In this paper we investigate in how far forces resulting from such processes affect BPTI. Finally, we address briefly the question in how far a cut-off for Coulomb forces, being dictated by numerical

necessity and being justified through screening effects, affects the configuration of BPTI within a molecular dynamics simulation.

The present paper addresses in Section 2 the methodological issue mentioned above, in Section 3 it applies some of the methods to BPTI in a continuum solvent. During several molecular dynamics simulations, each lasting 20 ps, we monitor the radius of gyration and the solvent accessible surface. Section 4 discusses the various methods and results as well as provides an outlook into future developments.

2 METHODS

2.1 *Basic Concepts*

To describe the dynamical behavior of large biopolymers one employs a semi-empirical force field for the non-electrostatic interactions. Electrostatic and semi-empirical force field together enable one to evaluate forces and integrate Newton's equations of motion (see [27, 28]).

To evaluate electrostatic interactions in biopolymers one needs to describe the electrostatic properties both inside and around a polymer. The charge distribution inside a polymer is obtained by a knowledge of the locations of all atoms within the polymer (which are usually derived from X-ray scattering data) and by assigning partial charges to all atoms. This procedure is described, for example, in [27]. In order to describe the motion of charged atoms and the effect of a solvent medium on this motion one needs to separate the intramolecular Coulomb forces between atomic partial charges of a polymer, which are accounted for by conventional molecular dynamics programs, from forces, usually referred to as the reaction field, which are due to effects of the solvent.

Thermodynamic equilibrium in a molecular dynamics simulation can be achieved by keeping the temperature at a desired value. This can be done by replacing the Newtonian equations by Langevin equations describing a heat bath (see [29, 3]) or by rescaling atomic velocities according to the definition of temperature,

$$T = \frac{1}{3k_B N} \sum_i m_i \langle v_i^2 \rangle_t. \tag{1}$$

In this expression k_B denotes the Boltzmann constant, N the number of atoms in the molecule, m_i the mass of the ith atom and v_i the absolute value of its velocity. By averaging over a time interval ($\langle\rangle_t$) fast term oscillations due to bond vibrations can be eliminated.

The size of a biopolymer is described by the radius of gyration

$$R_{gyr} = \frac{1}{N}\left(\sum_i (\mathbf{r}_i - \mathbf{r}_c)^2\right)^{1/2}, \tag{2}$$

where $\mathbf{r}_c$ is the center of geometry of the molecule, i.e., $\mathbf{r}_c = (1/N)\Sigma_i \mathbf{r}_i$. To estimate the extent to which the molecule is exposed to the solvent we determine the solvent accessible surface of the molecule by an algorithm developed by Lee and Richards [31].

2.2 *Protein in Solution: A Macroscopic Electrostatic Model*

2.2.1 *The Poisson–Boltzmann equation*

The electrostatic properties of biomolecules under physiological conditions are governed by the Poisson–Boltzmann equation [32]

$$\nabla\{\varepsilon(\mathbf{r})\nabla\Phi(\mathbf{r})\} - \bar{\kappa}^2(\mathbf{r})\frac{k_BT}{e}\sinh\left(\frac{e\Phi(\mathbf{r})}{k_BT}\right) = -4\pi\rho(\mathbf{r}) \tag{3}$$

Here e denotes the elementary charge, k_B the Boltzmann constant and T temperature. In the limit that the ionic strength of the solution is small, i.e., in case $|e\Phi(\mathbf{r})/k_BT| \ll 1$, Equation (3) can be approximated by the linearized Poisson–Boltsmann equation

$$\nabla\{\varepsilon(\mathbf{r})\nabla\Phi(\mathbf{r})\} - \bar{\kappa}^2(\mathbf{r})\Phi(\mathbf{r}) = -4\pi\rho(\mathbf{r}). \tag{4}$$

This partial differential equation can be solved analytically only for problems with spherical symmetry in $\varepsilon(\mathbf{r})$ and $\bar{\kappa}(\mathbf{r})$. Such solutions have been derived by Tanford and Kirkwood for a model dielectricum to explain protein titration curves [33, 34]. The model assumed a spherical region with low dielectric constant and point charges representing the charge distribution of the molecule. The peripheral region was assumed to be a region with high dielectric constant representing water. This region may contain solvated ions which implies a non-vanishing Debye–Hückel parameter $\bar{\kappa}$ in Equation (4).

For arbitrarily shaped dielectric discontinuities, i.e., in case of discontinuities at the boundary of a macromolecule, Equation (4) needs to be solved numerically. The analytical solution of Tanford and Kirkwood for spherical molecules (cavities) [33, 34] can be used to test the quality of any numerical algorithm developed for that purpose. We provide the Tanford and Kirkwood solution in Appendix A along with the corresponding Greens function [1]. The latter function allows one to determine solutions for any continuous charge distribution inside as well as outside of a spherical dielectric cavity. To our knowledge this Greens function has not been stated explicitly before.

2.2.2 *Finite difference approach*

A finite difference method is used to solve the linearized Poisson–Boltzmann Equation (4) numerically. The method was suggested by Warwicker and Watson [13] and then applied and modified by many others [35, 7, 36, 14]. An approach based on a distribution of induced polarization charge at the dielectric interface was proposed by Zauhar and Morgan [15]. The algorithm presented here is similar to the one used by Klapper *et al.* [7]. In this algorithm, the continuous functions $\Phi(\mathbf{r})$, $\varepsilon(\mathbf{r})$ and $\kappa(\mathbf{r})$ are defined on a cubic grid. To improve the accuracy of the representation of the dielectricum, we assign a separate value of the dielectric constant to the six faces of a grid cell rather than to the centers of the cells. Therefore, three times more data (each cell is shared by two adjacent cells) are required to represent the dielectric function $\varepsilon(\mathbf{r})$ than to represent the potential $\Phi(\mathbf{r})$ and the Debye–Hückel parameter $\bar{\kappa}(\mathbf{r})$. The relationship between the Debye–Hückel parameter and the ionic strength I of the solvent is given by

$$\kappa^2 = 8\pi N_A e^2 I/1000\varepsilon k_B T \tag{5}$$

where N_A is Avogadro's constant, e the elementary charge, ε the dielectric constant of the solution.

To discretize Equation (3) on a cubid grid, we integrate over the volume V_0 of a grid cell

$$\int_{V_0} \nabla\varepsilon(\mathbf{r})\nabla\Phi(\mathbf{r})d^3r - \int_{V_0} \bar{\kappa}^2(\mathbf{r}) \frac{k_BT}{e} \sinh\left(\frac{e\Phi(\mathbf{r})}{k_BT}\right) d^3r = -4\pi \int_{V_0} \rho(\mathbf{r})d^3r. \quad (6)$$

The integral on the r.h.s. yields $-4\pi Q_0$, where Q_0 is the total charge inside the grid cell. The first term on the l.h.s. can be transformed to a surface integral using Gauss' theorem. The finite difference representation of this integral can be written

$$\oint_{S_0} \varepsilon(\mathbf{r})\nabla\Phi(\mathbf{r}) \cdot \mathbf{n}da = \sum_{i=1}^{6} \varepsilon_i(\Phi_i - \Phi_0)h, \quad (7)$$

where $\mathbf{n}$ denotes the normal vector of the surface S_0 of the central grid cell, Φ_0 the potential at the center of a grid cell, and $\Phi_i (i = 1, 2, \ldots, 6)$ the potential at the centers of the six neighboring grid cells. ε_i is the value of the dielectric constant assigned to the cube face between the central grid cell and the cell with index i, and h denotes the length of the edge of a grid cell. We simplify the second term on the l.h.s. of Equation (6) as follows

$$\int_{V_0} \bar{\kappa}^2(\mathbf{r}) \frac{k_BT}{e} \sinh\left(\frac{\varepsilon\Phi(\mathbf{r})}{k_BT}\right) d^3r = \bar{\kappa}_0^2 h^3 \frac{k_BT}{e} \sinh\left(\frac{e\Phi_0}{k_BT}\right). \quad (8)$$

Here $\bar{\kappa}_0$ represents the modified Debye–Hückel parameter for the central grid cell related to the Debye–Hückel parameter κ_0 by $\bar{\kappa}_0 = \varepsilon_0^{1/2}\kappa_0$. Combining (6), (7), (8) the relation

$$\sum_{i=1}^{6} \varepsilon_i(\Phi_i - \Phi_0) - \bar{\kappa}^2 \frac{k_BT}{e} \sinh\left(\frac{e\Phi_0}{k_BT}\right) + 4\pi Q_0/h = 0 \quad (9)$$

is obtained.

In case of low ionic strength, i.e., $|\Phi(\mathbf{r})/k_BT| \ll 1$, the sinh ( ) term in Equation (8) can be linearized. Because $\kappa(\mathbf{r})$ assumes a constant value in the solvent region and vanishes in the interior of the molecule, in the linearized form of Equation (8) Φ_0 represents the average value of the potential in the central grid cell. The linearization of Equation (8) replaces Equation (9) by the well-known equation

$$\Phi_0 = \frac{\sum_{i=1}^{6} \varepsilon_i\Phi_i + 4\pi Q_0/h}{\sum_{i=1}^{6} \varepsilon_i + \bar{\kappa}_0^2 h^2}, \quad (10)$$

referred to as the discrete linearized Poisson–Boltzmann equation (see [7]).

2.2.3 *Boundary condition*

Equation (10) can be solved iteratively by choosing appropriate initial values for $\Phi(\mathbf{r})$ at all grid cell centres and evaluating the potential repeatedly by using Equation (10). For this purpose, values need to be specified at the boundaries of the grid. The natural boundary condition of the problem is that $\Phi(\mathbf{r})$ vanishes on a boundary at very large distances from the polymer. Such choice is computationally unfeasable. However, one can also choose a boundary condition at a closer boundary if the values of $\Phi(\mathbf{r})$ are known there. Our strategy is to employ such a boundary and to choose approximate values of $\Phi(\mathbf{r})$ on this boundary (see [7]). The simplest approximation would be to

assign vanishing potential values to all centres of cells at the boundary of the grid. A better approximation is furnished by the potential values at the boundary which would hold for a homogeneous Debye–Hückel dielectricum, namely

$$\Phi_i = \sum_j \frac{q_i \exp(-\kappa r_{ij})}{\varepsilon r_{ij}} \tag{11}$$

where r_{ij} is the distance of the ith boundary grid point to the jth partial atomic charge, where ε is the dielectric constant and κ the Debye-Hückel parameter of the external medium.

2.2.4 *Multigrid method*

The scheme of updating Φ employed by us is the symmetric Gauss–Seidel iteration [37]. To speed up convergence a multigrid method has been applied. The algorithm starts on a coarse grid of 4×4 cells. On this level of resolution, the system of linear equations corresponding to Equation (10) can be solved explicitly. Using interpolated values from the coarse grid as initial guesses on an $8 \times 8 \times 8$ grid, iteration steps are performed until the potential changes by less than a certain fraction. We have chosen the value 10^{-4} for this fraction. The same procedure is repeated for a $16 \times 16 \times 16$ grid. The grid is shown schematically in the left part of Figure 1. In the next step, the grid is refined by a factor of two only in the region containing the protein. The corresponding grid is shown in the middle part of Figure 1. In the region external to the polymer a coarse grid is employed. The iteration procedure is now applied to both parts of the grid. At the boundary between the two parts of the grid linear interpolation is used to link the potential values on the coarse grid to the potential values on the fine grid and vice versa. After convergence is achieved (criterion see above) the inner grid is refined again by a factor of two and a final relaxation procedure is carried out. The corresponding grid is shown in the right part of Figure 1. The grid width is now $h = 1$ Å on the inner grid.

2.2.5 *Overrelaxation method*

The algorithm can be made more efficient using the method of successive overrelaxation (SOR, see [37]) provided that an optimal value for the overrelaxation parameter ω is chosen. To evaluate the speed-up of the algorithm due to successive overrelaxation, we solved the two problems described in Section 2.2.8 for a series of 20 different values of the overrelaxation parameter ($1 \leqslant \omega < 2$). In case of a point charge in vaccuum

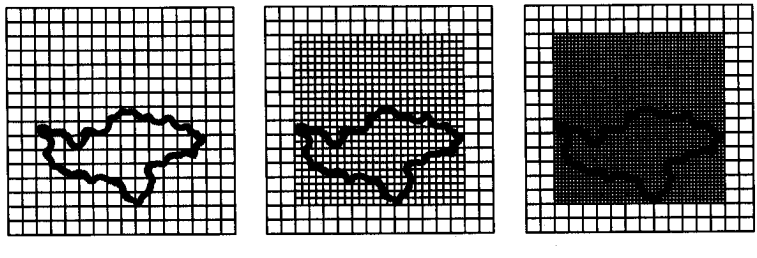

Figure 1 Schematic representation of three different stages of the *heterogeneous discretization* employed by us according to Section 2.2.4 for evaluation of the potential $\delta\Phi(\mathbf{R}_{ijk})$. The protein surface is marked by a thick line. The resolution of the discretization lattice with grid cell centers at $\mathbf{R}_{ijk}$ is fine in a region containing the protein and is coarse in the remaining space.

(see Section 2.2.8 for details), the algorithm was faster by a factor of 1.9 using an overrelaxation parameter of $\omega = 1.5$. In case of a dipole in the center of a dielectric sphere (see Section 2.2.8), the algorithm was accelerated by a factor of 5.6 for $\omega = 1.2$.

2.2.6 *Full multigrid method*
An even faster algorithm should result from a full multigrid method (FMG) as described in [38]. This method uses so-called *multigrid cycles* (MGC) on a series of grids with gradually increasing resolution. A multigrid cycle can be described as follows: at a certain resolution convergence is achieved by gradually proceeding to coarser grids until the coarsest grid, i.e., the resolution the multigrid algorithm was started with, is reached; on each grid, only a few iteration steps are performed. After iterating on the coarsest grid, one gradually goes back to finer grids until the finest grid, is reached again; the transition between grids of different resolution is managed by employing linear interpolation. For details and for the theory of multigrid methods see [39, 40]. The use of multigrid cycles instead of the usual relaxation method is likely to increase the performance of the algorithm to solve the electrostatic field of proteins by a large margin.

2.2.7 *Modeling electrostatics of a protein*
The charges Q_i at the centers of the grid cells are obtained by distributing the partial atomic charges q_j of all atoms of a protein using a tri-linear weighting function as suggested in [7]. This procedure distributes partial atomic charges between several grid cells in order to preserve the maximum number of moments of the charge distribution of the protein.

A map of surface points of the molecule is determined by using the algorithm of Connolly [41]. Grid cells containing any surface points and cells within the surface are considered as part of the protein interior, all other grid cells are regarded as part of the solvent. The dielectric constant is set to $\varepsilon = 80$ in the solvent and to $\varepsilon = 2$ in the protein region. The Debye–Hückel parameter is set to $\kappa = 0.125\,\text{Å}^{-1}$ in the solvent, corresponding to a physiological ionic strength of 150 mM, and to $\kappa = 0$ in the protein interior. The orientation of the protein relative to the grid and the spacing of the grid are chosen with respect to a minimum distance of 1.5 Debye lengths κ^{-1} (corresponding to about 12Å at physiological ionic strength) between the surface of the protein and the boundary of the grid.

2.2.8 *Separating Coulomb and screening potential*
To test the accuracy of our algorithm we compared the numerical results for two simple problems with their analytical solutions. The first problem considered is the case of a point charge in vacuum ($\varepsilon = 1, \kappa = 0$). The relative error between the exact Coulomb potential and two different kinds of numerical solutions is shown in Figure 2. The point charge is located in the center of a grid cell. A solution using a homogeneous grid ($64 \times 64 \times 64, h = 1$ Å) and another using a heterogeneous grid (lower resolution within a distance of 8 Å from the grid boundary, i.e., beyond grid cell with index 24) are compared there. In both cases, the error is larger than one percent only within four grid cells around the point charge. Using a lower resolution of the grid in the boundary region does not reduce accuracy considerably. However, near the point charge, the error increases above 8 percent. If the location of the charge were nearer to the edge of a grid cell, the error at this location would be even larger (up

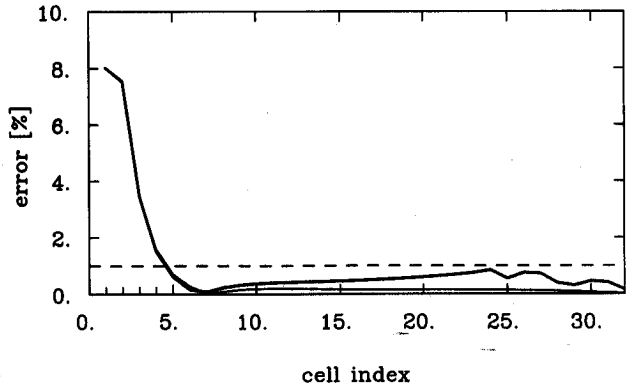

Figure 2 Relative error between the numerical solution of the linearized Poisson–Boltzmann equation for a point charge in vacuum and the exact Coulomb potential q/r. The algorithm and boundary conditions assumed are explained in Section 2.2.2–2.2.4. The position of the point charge is in the center of a cell with index $j = 0$. The thick line denotes the error in the case of the *heterogeneous discretization* (see Figure 1), which implies a lower resolution beyond the cell with $j > 24$ i.e., $h = 1$ Å in the central region and $h = 4$ Å in the peripheral region. The thin line shows the error in the case of a grid with homogeneous resolution ($h = 1$ Å). The space in which the potential was evaluated is a cube with edges of 64 Å length. The cell with index $j = 0$ is located in the center of the cube. The horizontal dashed line marks the 1% error limit. ($\varepsilon = 1, \kappa = 0$)

to 50 percent). Therefore, even in homogeneous media without dielectric interfaces, the potential is represented poorly near singularities.

If one wishes to account in a molecular dynamics simulation for the effect of an external solvent, an accurate representation of the forces in the interior of a macromolecule is needed. The method described above appears to be unsuitable in this respect. The reason for the failure is the existence of singularities of the potential at the position of partial atomic charges which are represented poorly. This deficiency can be corrected, in one splits the potential $\Phi(\mathbf{r})$ into two terms

$$\Phi(\mathbf{r}) = \sum_j \frac{q_j}{\varepsilon_m |\mathbf{r} - \mathbf{r}_j|} + \delta\Phi(\mathbf{r}) \tag{12}$$

The first term represents the Coulomb potential in a homogeneous medium with dielectric constant within the protein. This term contains all the singularities due to the Coulomb potentials of the partial atomic charges q_j at $\mathbf{r}_j$. $\delta\Phi(\mathbf{r})$ represents the modification of the Coulomb term due to screening by the aqueous environment. The merit of the decomposition given by (12) lies in the fact that the screening contribution $\delta\Phi$ to the potential Φ actually can be evaluated numerically.

The screening potential and the corresponding force field $\nabla\delta\Phi(\mathbf{r})$ plays a crucial role for the motion of atoms in a continuous dielectric and Debye–Hückel medium in that it furnishes the so-called reaction field which describes the forces which the solvent exerts on the atomic partial charges of a polymer. The separation in Equation (12) in the context of a molecular dynamics simulation implies that intramolecular Coulomb forces are evaluated through a conventional molecular dynamics algorithm whereas the effect of the solvent is attributed to the reaction field $\nabla\delta\Phi$.

The procedure developed in [1] to evaluate $\delta\Phi$ will be described now. We consider

the representation

$$\Phi(\mathbf{r}) \approx \sum_j \frac{q_j}{\varepsilon_m |r - r_j|} + \Phi_A(\mathbf{r}) - \Phi_B(\mathbf{r}) \tag{13}$$

where $\Phi_A(\mathbf{r}) \approx \Phi(\mathbf{r})$ and $\Phi_B(\mathbf{r}) \approx \Sigma_j q_j/\varepsilon_m|\mathbf{r} - \mathbf{r}_j|$ are numerical approximations obtained by applying the finite difference algorithm described in Section 2.2.2. $\Phi_A(\mathbf{r})$ and $\Phi_B(\mathbf{r})$ are evaluated as follows:

1. $\Phi_A(\mathbf{r})$ is determined by solving the linearized Poisson–Boltzmann equation numerically for a heterogeneous problem with a low dielectric constant ε_m and partial atomic charges in the molecular region, a high dielectric constant ε_w and a non-vanishing Debye–Hückel parameter κ in the peripheral region.
2. $\Phi_B(\mathbf{r})$ is obtained by solving the linearized Poisson–Boltzmann equation numerically for a homogeneous problem with partial atomic charges at the same locations and of the same kind as above and for the same low dielectric constant ε_m, however, assumed in the whole grid volume. The Debye–Hückel parameter vanishes everywhere.
3. By comparing Equation (13) with Equation (12) the screening contribution $\delta\Phi(\mathbf{r})$ is approximated by

$$\delta\Phi(\mathbf{r}) = \Phi_A(\mathbf{r}) - \Phi_B(r). \tag{14}$$

By evaluating the potential $\Phi(\mathbf{r})$ using Equation (13) the error due to the inaccuracy of the finite difference algorithm near partial atomic charges is reduced considerably by cancellation of this error in Φ_A and Φ_B. An approach similar to that adopted here and in [1] was used by Gibson and Honig [21] to determine the effect of an external solvent on the total electrostatic energy of a protein.

To check the accuracy of the method suggested above we considered a dipole of two point charges 1 Å apart and centered in a dielectric sphere (R = 20 Å) with low

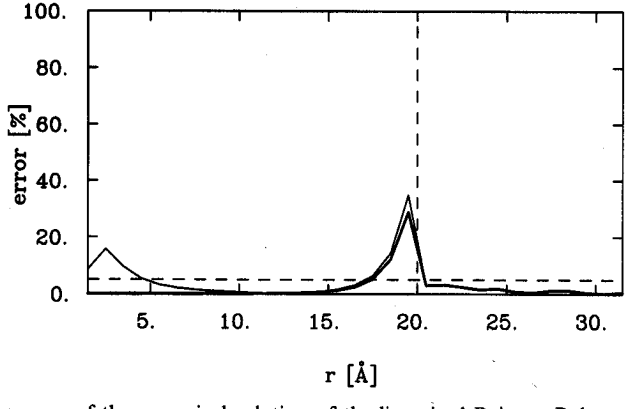

Figure 3 Relative error of the numerical solution of the linearized Poisson–Boltzmann equation for a dipole consisting of two point charges 1 Å apart. The dipole is centered inside a sphere with low dielectric constant (ε_m = 2) and radius R = 20 Å (indicated by vertical dashed line). The sphere is surrounded by a medium with high dielectric constant (ε_w = 80). The medium is a cube with edges of 64 Å length. The grid spacing is h = 1 Å. The thin line shows the error resulting from the calculation described in Section 2.2.2–2.2.4, the thick line shows the error obtained when the superposition principle (see Section 2.2.8) is employed. The horizontal dashed line marks the 5% error limit. ($\kappa_i = \kappa_0 = 0$, i.e., no Debye–Hückel screening)

dielectric constants ($\varepsilon_m = 2$). The sphere is located in a cubic grid (size 64 Å, $h = 1$ Å) and is surrounded by a medium with high dielectric constant ($\varepsilon_w = 80$). The medium does not contain any ions ($\bar{\kappa} = 0$). The problem was solved by applying two different kinds of numerical algorithms. Figure 3 shows that the ordinary finite difference algorithm as described in Section 2.2.2 produces an error larger than 15 percent (as in the case of Figure 2 the error would be larger if the point charges were located near the edges of a grid cell), whereas the algorithm based on Equation (13) reproduces the exact result near the point charges (at $r = 0$) with an accuracy better than 5 percent. Near the dielectric boundary (indicated by the vertical dashed line) the algorithm based on Equation (13) produces an error with a maximum value of less than 30 percent while the ordinary finite difference algorithm produces a maximum error of about 35 percent.

2.2.9 *Poisson–Boltzmann equation for screening potential*

An alternative method to apply the decomposition (12) is to evaluate $\delta\Phi(\mathbf{r})$ directly. A differential equation $\delta\Phi(\mathbf{r})$ is obtained by subtracting from the linearized Poisson Boltzmann equation

$$\nabla(\varepsilon(\mathbf{r})\nabla(\Phi_C\mathbf{r}) + \delta\Phi(\mathbf{r}))) - \bar{\kappa}^2(\mathbf{r})(\Phi_C(\mathbf{r}) + \delta\Phi(\mathbf{r})) = -4\pi\rho(\mathbf{r}) \tag{15}$$

the Poisson equation

$$\nabla\varepsilon_m\nabla\Phi_C(\mathbf{r}) = -4\pi\rho(\mathbf{r}) \tag{16}$$

to yield

$$\nabla\varepsilon(\mathbf{r})\nabla\delta\Phi(\mathbf{r}) - \bar{\kappa}^2(\mathbf{r})\delta\Phi(\mathbf{r}) = -4\pi\tilde{\rho}(\mathbf{r}). \tag{17}$$

Equation (15) is the partial differential equation for the heterogeneous system, where the potential $\Phi(\mathbf{r})$ has been split according to Equation (12), which implies

$$\Phi_C(\mathbf{r}) = \sum_j \frac{q_j}{\varepsilon_m|\mathbf{r} - \mathbf{r}_j|}. \tag{18}$$

$\tilde{\rho}(\mathbf{r})$ is an effective charge distribution defined by

$$\tilde{\rho}(\mathbf{r}) = \frac{1}{4\pi}(\nabla(\tilde{\varepsilon}(\mathbf{r})\nabla\Phi_C(\mathbf{r}) - \tilde{\kappa}^2(\mathbf{r})\Phi_C(\mathbf{r})), \tag{19}$$

where

$$\tilde{\varepsilon}(\mathbf{r}) = \varepsilon(\mathbf{r}) - \varepsilon_m = \begin{cases} 0 & \text{in the molecular region} \\ \varepsilon_w - \varepsilon_m & \text{in the solvent region} \end{cases} \tag{20}$$

Equation (17) is a linearized Poisson–Boltzmann equation for the potential $\delta\Phi(r)$. It can be discretized and solved numerically as described in Section 2.2.2.

To solve Equation (17) by discretization one has to determine the charges Q_j assigned to the cells of the lattice. When integrating the charge density $\tilde{\rho}(\mathbf{r})$ over the volume V_0 of a grid cell (see Equation (9)), one obtains

$$Q_0 = -\oint_{S_0}\tilde{\varepsilon}(\mathbf{r})\nabla\Phi_C(\mathbf{r})\cdot\mathbf{n}da + \int_{V_0}\bar{\kappa}^2(\mathbf{r})\Phi_C(\mathbf{r}). \tag{21}$$

The first term on the r.h.s. of (21) gives an important contribution confined to grid

cells at the interface between the molecule and the solvent. The resulting charges Q_0 are the polarization charges which describe the effect of the discontinuity of the dielectric constant. For grid cells entirely inside the polymer region, Q_0 vanishes since both $\tilde{\varepsilon}(\mathbf{r})$ and $\tilde{\kappa}(\mathbf{r})$ vanish in this region. For grid cells entirely in the solvent region the first term of (21) does not contribute since $\tilde{\varepsilon}(\mathbf{r})$ is constant there, and since the surface integral over $\nabla\Phi_C$ vanishes according to Gauss' theorem applied to Equation (16).

Appropriate boundary values can be obtained by superimposing the boundary conditions for Equation (15) which are given by Equation (11) with the boundary conditions for the Poisson Equation (16) to yield the boundary condition

$$\delta\Phi_i = \sum_j \frac{q_j}{r_{ij}} \left(\frac{1}{\varepsilon_w} \exp(-\kappa r_{ij}) - \frac{1}{\varepsilon_m} \right), \tag{22}$$

where r_{ij} is the distance between the ith boundary grid point and the jth partial atomic charge in the original system.

Due to the fact that $\tilde{\rho}(\mathbf{r})$ vanishes inside the polymer, we expect a numerical solution for $\delta\Phi$ to be very smooth in that region and, therefore, to be numerically accurate. We currently implement the suggested algorithm for $\delta\Phi$ into our electrostatics program to obtain a numerically improved description of electrostatic potentials inside proteins. The results presented below, however, were obtained without this algorithm.

2.3 *Positioning of Counter-Charges at the Protein Surface*

Often biological macromolecules carry a net charge. The charge in case of a protein is determined by the pK_A-values of amino acid side chains which often are modified by local interactions and are not known. When modeling the electrostatic properties of such a system it may be necessary to neutralize the system to render it stable in a molecular dynamics simulation. An example is double-stranded DNA which requires neutralization of charges on its phosphor groups by external ions [42, 43]. This neutralization is due to either protonation or deprotonation or due to binding of external ions to the molecular system.

To estimate the effect of neutralization of a molecule we place counter-charges in the solvent near the surface of the molecule to achieve local electrostatic neutrality. The counter-charges are placed at positions of minimal electrostatic energy. We want to describe now how these positions have been determined by us. The procedure is explained using the protein BPTI as an example.

In order to identify such positions on the surface of BPTI, which carries a net charge of +6, we used the following method:

1. In a first step the molecule is surrounded by a sphere which is centered at the geometric center of the molecule and which encloses the molecule entirely, i.e., the sphere should not touch the molecule. We choose the closest distance between this sphere and the molecule to be 4 Å. In the case of BPTI, the radius of the corresponding sphere is 25 Å.
2. In a second step we select 2000 evenly distributed points on the sphere obtained in step 1.
3. In a third step a test charge (negative sign in case of BPTI with a van der Waals radius of 2.5 Å is placed at each point of the set chosen in step 2 and an energy minimization is carried out by allowing the test charge to move towards BPTI. The atoms of BPTI are fixed during minimization, i.e., only the test charge

moves. After the minimization procedure has converged the total energy (electrostatic energy plus van der Waals energy) of the test charge at its new position is evaluated. The large number of initial positions for the counter-charges on the sphere leads to a much smaller number of optimal positions near the surface of the polymer, i.e., test charge starting at different initial positions ends up in the same minimum. In the case of BPTI, 2000 initial positions ended up in 80 minima.

The electrostatic interaction energy between counter charge and protein is a measure for the binding strength of that charge. Positions with considerably negative interaction energies favouring binding are referred to as *hot spots*. Depending on the net charge of the polymer and on the number of hot spots one can choose a certain number of counter charges to be added to the system. In the case of BPTI, we wanted to neutralize the molecule, hence, six positions for counter-charges had to be chose.

4. In a fourth step the following procedure was used to place six counter charges at six of the 80 hot spots: The first charge was placed at the location with the lowest total energy. The other charges were added to the system successively. Each charge was placed at the one of the remaining hot spots which had the lowest energy, taking into account the effect of the counter-charges already present in the system.

2.4 *Molecular Dynamics Simulation of BPTI*

Molecular dynamics simulation methods have been extensively described and applied by many authors [44, 16, 45, 46, 47, 17, 48, 49, 50]. In our investigations we used the program X-PLOR [51] derived from CHARMM [27]. Starting from the X-ray structure of BPTI by Deisenhofer and Steigemann [52], the BPTI molecule was prepared for our molecular dynamics simulations by the following steps:

1. An energy minimization using the conjugate gradient method (see [28]) has been carried out. We used for this purpose the Powell algorithm of X-PLOR [51].
2. The molecule has been heated to 300 K by gradually rescaling atomic velocities to higher values while doing a molecular dynamics simulation.

The four simulations described in Section 3 were based on the structure resulting from these steps. All four simulations lasted 20 ps and consisted of two periods, an *equilibration period* lasting 10 ps and an *analysis period* also lasting 10 ps. The periods are somewhat briefer than in conventional molecular dynamics calculations not accounting for solvent screening effects, the reason being the very large computational effort involved in solving repeatedly the Poisson–Boltzmann equation. During the *equilibration period* of the simulations the atomic velocities were rescaled every 250 fs to maintain, according to Equation (1), a temperature of 300 K. During the *analysis period* velocities were not rescaled, except in case of the one simulation which accounted for the effect of solvent screening. The need for the latter rescaling is explained further below. To eliminate fast oscillations due to hydrogen bond vibrations, hydrogen bonds were kept at fixed length using the so-called SHAKE algorithm [17]. This allowed us to use a time step of 1 fs for the integration of Newton's equations.

To incorporate the effect of solvent screening into molecular dynamics simulations the *screening potential* $\delta\Phi(\mathbf{r})$ defined in Equation (12) is used to obtain the contribu-

tion to the atomic force field due to screening, i.e., the reaction field $\nabla\delta\Phi(\mathbf{r})$ is added to the conventional (Charmm [27]) force field. This potential is non-singular and is well-defined at the locations of the protein atoms. Therefore, the additional force acting on an atom with partial charge q_j due to screening by the solvent is

$$F_j = -q_j \frac{\partial}{\partial \mathbf{r}_j} \delta\Phi(\mathbf{r}_j). \tag{23}$$

The problem in applying (23) is that $\delta\Phi(\mathbf{r})$ is represented in the numerical solution only on a discrete lattice. We will now explain how a suitable continuum representation, for which the gradient can be evaluated, is found.

Using the potential $\delta\Phi(R_{ijk})$ on a grid with positions R_{ijk} obtained by the numerical method above for a certain configuration of the protein, a continuous potential $\delta\Phi(\mathbf{r})$ is constructed by linear interpolation. Since such $\delta\Phi(\mathbf{r})$ is not differentiable everywhere, it cannot be used to construct a force field according to Equation (23). The following method is applied instead (see [1]):

1. Let $\delta\Phi_{ijk}$ be the screening potential at grid point $(X_{ijk}, Y_{ijk}, Z_{ijk})$ where the indices i, j and k correspond to the direction of the x-, y- or z-coordinates, respectively, and where h is the distance between neighboring grid points. We then use $F^x_{ijk} = (\delta\Phi_{i+1,jk} - \delta\Phi_{ijk})/h$ as an approximation for the x-component of $\nabla(\delta\Phi)$ at position $(X_{ijk} + h/2, Y_{ijk}, Z_{ijk})$. F^y_{ijk} and F^z_{ijk} can be obtained and used in a similar way.
2. The three force components are defined on grids which are shifted by a distance of $h/2$ in the direction of the x, y- or z-coordinate with respect to the grid $(X_{ijk}, Y_{ijk}, Z_{ijk})$. The force F_j on atom j at position $\mathbf{r}_j$ can be obtained by tri-linear interpolation on the latter grid.

In our investigations the reaction field determined as described was used in a molecular dynamics simulation of BPTI in addition to conventional intramolecular binding forces, van der Waals forces and Coulomb forces. During the simulation the potential $\delta\Phi$ was updated every 250 fs. A faster schedule of updating seemed unnecessary due to the large time constant $\tau = 10\,ps$ [32] of orientational dielectric relaxation of water. This long relaxation time implies that the solvent, compared with the rapidity of BPTI motions, adapts only very slowly to charge rearrangements of the protein by altering $\delta\Phi$. In our simulation, we accepted every 250 fs abrupt changes of the new screening potential $\delta\Phi$.

The total energy of the system can be divided into the three contributions

$$E_{\text{total}} = E_{\text{internal}} + E_{\text{screening}} + E_{\text{solvent}}. \tag{24}$$

Here E_{internal} contains the energy contributions for all internal degrees of freedom as defined in [27], $E_{\text{screening}}$ describes the interaction of atomic partial charges with the screening potential

$$E_{\text{screening}} = \frac{1}{2}\sum_j q_j \delta\Phi(\mathbf{r}_j), \tag{25}$$

and E_{solvent} is the internal energy of the solvent. This latter energy has not been evaluated by us.

The energy of the simulated protein defined as

$$E_{\text{protein}} = E_{\text{internal}} + E_{\text{screening}} \tag{26}$$

is not conserved, the change in E_{protein} being transferred to E_{solvent}. The exchange of energy leads to a change of temperature of the protein. We have applied the rescaling method mentiond in Section (2.1) to keep the temperature constant. This procedure accounts for the fact that dielectric heating and cooling of the solvent would be followed by exchange of kinetic energy between protein and solvent.

2.5 *Accounting for finite dielectric relaxation times and ion mobilities*

The following approach allows one to account for a finite dielectric relaxation time and finite ion mobilities of the solvent. We redefine the screening potential such that only a fraction of the change of $\delta\Phi$ as defined in (14) is accepted at each updating step. The screening potential $\delta\Phi$ is updated at times δt, $2\delta t$, $3\delta t$, . . . , $n\delta t$. Let $\delta\phi(t + \delta t)$ be the difference between the old screening potential determined at time t and the new one determined at time $t + \delta t$

$$\delta\phi(t + \delta t) = \delta\Phi(t + t) - \delta\Phi(t). \tag{27}$$

$\delta\phi(t + \delta t)$ would be the change in the screening potential which would occur if the solvent reacts instantaneously to rearrangements of the charges of the protein at time $t + \delta t$. Because the time constant τ for orientational dielectric reorientation is large compared to the time step of 1 fs used in our molecular dynamics simulation, the solvent appears very inert in its configurational adjustment. This behaviour can be described by a relaxation factor $1 - \exp(-\delta t/\tau)$ which gives the fraction of $\delta\phi(t + \delta t)$ that actually occurs in the time δt between two updates of the screening potential. The modified screening potential $\delta\Phi(t + \delta t)$ which takes into account the inertia of the solvent is then calculated according to

$$\delta\Phi(t + \delta t) = \delta\Phi(t) + (1 - \exp(-\delta t/\tau))\delta\phi(t + \delta t). \tag{28}$$

We are currently implementing this scheme into our molecular dynamics description of proteins in dielectric media.

One may alternatively update the charge density $\rho(\mathbf{r})$ defined in Equation (19) by a corresponding scheme. This approach would allow one to separately deal with the contributions due to the dielectric response of the solvent, i.e., ε_w, and due to the response of screening through ionic motion, i.e., κ, which, in principle, are governed by two different relaxation times.

3 RESULTS

The aim of our study has been to demonstrate that molecular dynamics simulations accounting for electrostatic solvent effects are feasible. We also wanted to determine to which extent a solvent affects structure and dynamics of a protein. For this purpose we have carried out four different molecular dynamics simulations of BPTI, each lasting a period of 20 ps. The relatively brief simulation periods are due to the fact that the necessary repeated solution of the Poisson–Boltzman equation are very time-consuming.

As explained above, the four simulations each entail two periods, namely an *equilibration period* lasting 10 ps and an *analysis period* also lasting 10 ps. (see Section 2.4). The four simulations will be referred to as *simulations A, B, C* and *D*. All four simulations started from the same structure of BPTI at 300 K, which was obtained as described in Section 2.4.

Simulation A described in Section 3.1 takes into account all electrostatic interactions within the protein, but neglects the influences of solvent screening or counter charges. This simulation serves as a reference against which other simulations can be compared. *Simulation B,* in addition to the forces accounted for by *simulation A,* includes forces due to solvent screening, the latter being determined using the finite difference algorithm presented in Sections 2.2.2, 2.4, and 3.2. In *Simulation C* we investigate the effect of counter charges. Such charges arise due to protonation/deprotonation controlled through the pK-values of surface amino acid side groups as well as due to binding of ions. This simulation is described in Section 3.3. Finally, *Simulation D* addresses the somewhat more methodological issue of the effect of a cut-off of Coulomb interactions on structure and dynamics. The simulation, described in Section 3.4, is the same as *simulation A* except that a cut-off range for the Coulomb forces is assumend. The parameters which define the *simulations A, B, C* and *D* are listed in Appendix B.

3.1 *Molecular Dynamics Simulation of* BPTI *in Vaccuum*

Simulation A was carried out in a homogeneous dielectric medium disregarding effects due to dielectric and Debye–Hückel screening by an external solvent. The effects due to the polarizability of the protein atoms were accounted for by a dielectric constant $\varepsilon = 2$. All electrostatic interactions between protein atoms were taken into account using algorithms provided by the molecular dynamics program. The time step of the integration was 1 fs. This long time step was possible because fast oscillations due to vibrations of hydrogen bonds were eliminated using the SHAKE algorithm [17] (see Section 2.4). Four water molecules present in the BPTI structure were represented using the ST2 water model which is implemented into CHARMM [27] and X-PLOR [51]. To suppress fast oscillations of bonds and angles within these water molecules the molecules were treated as rigid bodies, i.e., their internal degrees of freedom were neglected. The results obtained from *Simulation A* are compared with the ones of *simulations B, C* and *D* in the following sections and will not be discussed here separately.

3.2 *Molecular Dynamics Simulation of* BPTI *in Solution*

Simulation B is identical in all respects to *simulation A* except that additional forces, i.e., the reaction field, were accounted for which derive from the effect of an external solvent. The dielectric constant was $\varepsilon = 2$ inside the protein (like for *simulation A*) and $\varepsilon = 80$ in the solvent. The Debye–Hückel parameter was $\kappa = 0.125\,\text{Å}^{-1}$. The discretization lattice used for the finite difference algorithm had an initial resolution of 16 Å in a $4 \times 4 \times 4$ grid and a final resolution in the protein interior of 1 Å. The screening potential was updated every 250 fs without applying the relaxation mechanism described in Equation (28). Accordingly, there were abrupt transitions between successive potentials. Atomic velocities were rescaled every 250 fs not only during the *equilibration period,* but also during the *analysis period* of the simulation to avoid heating/cooling through the time-dependent solvent potential.

To demonstrate solvent effects we actually have carried out the first 5 ps of the simulation disregarding solvent effects, switching these effects on instantaneously at $t = 5$ ps. This procedure allows one to visualize the deviations between observables of 'solvated' and 'unsolvated' BPTI. A first observable considered is the absolute value of the total force acting on any one atom j averaged over all N atoms

$$\mathscr{F}(t) = \frac{1}{N}\sum_{j=1}^{N} |\mathbf{F}_j(t)|. \tag{29}$$

This quantity is compared with corresponding averages for various contributions to the total force, namely the Coulomb force between atoms and the forces due to dielectric and Debye–Hückel screening (reaction field). The time development of the quantities mentioned is shown in Figure 4 for the *analysis period* of *simulation B*. The figure shows that the mean total force exceeds the mean electrostatic force by a factor of 6 and the mean screening force (reaction field) by a factor of 30. In particular, the standard deviation of the total force with respect to the set of all atoms is much larger than the two electrostatic contributions. The large ratio between standard deviation of all forces and mean electrostatic force is due to the fact that short range potentials like harmonic and van der Waals potentials vary considerably more during vibrational periods of protein atoms than the electrostatic and screening potentials do. Moreover, the contributions due to Coulomb interactions and screening are underestimated to some extent compared to the other contributions because the average was calculated over all atoms, i.e., also neutral ones. Yet the ratio between the mean Coulomb force and the mean screening force (reaction field), namely a factor of 5, is appropriate since both averages include neutral atoms.

Figure 5 presents the time development of various contributions to the total energy for the last 5 ps of the *equilibration period* of *simulation B*, starting from the time when

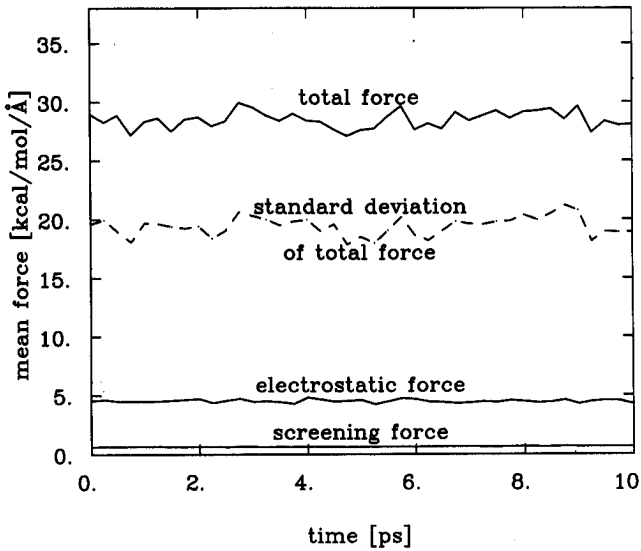

Figure 4 Time development of mean forces acting between atoms of BPTI for the second phase of molecular dynamics simulation B (see Section 3.2). The average is taken at every time step over the absolute values of the forces acting on all atoms in the protein. The solid line at the top shows the total mean force, the dashed line represents the standard deviation of the total force with respect to the set of all protein atoms. The solid line below denotes the mean electrostatic force due to Coulomb interactions within the protein. The line at the bottom of the diagram shows the contribution due to screening by the solvent. (Parameters for simulation B are in section 3.2, the discretization scheme used for evaluation of $\delta\Phi$ is defined in Section 2.2.4, parameters for the water continuum model are given in Section 2.2.7; see also Appendix B.)

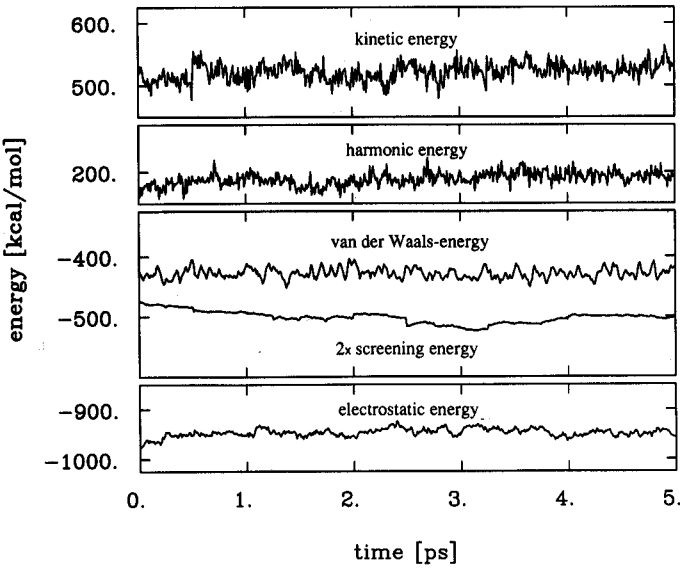

Figure 5 Time dependence of various contributions to the total energy of BPTI resulting from molecular dynamics simulation B as described in Section 3.2. The screening contribution is scaled by a factor of 2. In the simulation the screening potential $\delta\Phi(\mathbf{R}_{ijk})$ was updated and atomic velocities were rescaled (corresponding to $T = 300$ K) every 250 fs. Because of the coarse updating scheme the screening energy, defined as $E_{\text{screening}} = 1/2\,\Sigma_j \delta\Phi(\mathbf{r}_j(t))$ (see Equation (25) exhibits discontinuities. (Parameters for simulation B are in Section 3.2, the discretization scheme used for evaluation of $\delta\Phi$ is defined in Section 2.2.4, parameters for the water continuum model are given in Section 2.2.7; see also Appendix B.)

the screening potential has been switched on. During the first ps of the equilibration the kinetic energy and the harmonic energy are increasing slightly as the protein adapts to the solvent. The electrostatic energy is decreasing by a small amount for the same reason. The screening energy, scaled by a factor of 2 in our diagram, exhibits a relaxation behaviour towards a lower level. This energy drops by about -25 kcal/mol and then rises again by about 12 kcal/mol to reach an average solvation energy of about -250 kcal/mol. We have ommitted in Figure 5 the energies during the *analysis period* of *simulation B* since during this period the screening energy remained at values around -250 kcal/mol reflecting a stationary state.

One can readily notice in Figure 5 discontinuities of the screening energy which are due to the sudden updates of the screening potential. Obviously, the slow time of $\tau = 10$ ps for orientational dielectric relaxation of water is inconsistent with the fast changes of the screening potentials. To improve this deficiency one should update the screening potential according to the potential given in Equation (28) which assumes an exponential relaxation process with a proper relaxation time. Such procedure would eliminate the discontinuities discernable in Figure 5.

To estimate the influence of the screening forces (reaction field) on the overall shape of the molecule, we considered two different properties of BPTI, namely the radius of gyration, a measure for the size of the molecule (see Section 2.1), and the solvent accessible surface, a measure for the "wrinkling" of the surface. The latter property has been determined by the method of Lee and Richards [31].

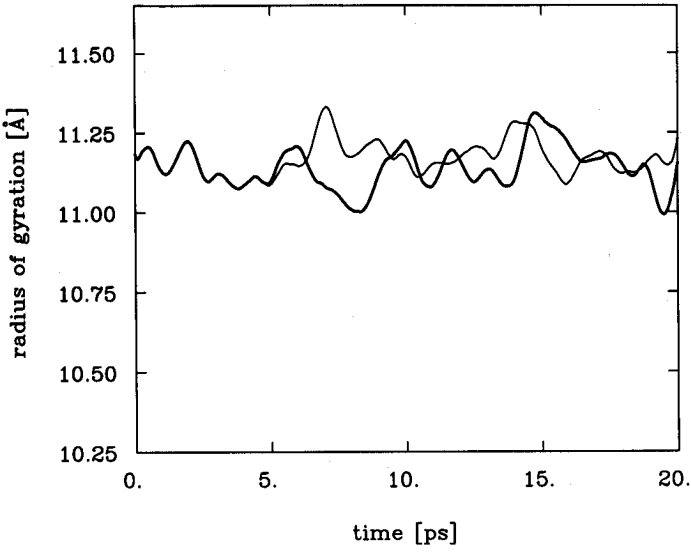

Figure 6 Time development of the radius of gyration of BPTI for molecular dynamics simulations A and B. The radius of gyration is used as a measure for protein size. The thick line refers to simulation A (protein in vacuum, full range electrostatic interactions are taken into account, parameters see Section 3.1), the thin line refers to simulation B (protein in solution, parameters for simulation and discretisation see Section 3.2 and 2.2.4). Both simulations started with the same protein structure (see definition of simulations A and B in Section 3.1 and 3.2). In simulation B, screening was switched on instantaneously at $t = 5$ ps.

Figure 6 presents the time-dependence of the radius of gyration R_{gyr} resulting from *simulation A* and from *simulation B*. The simulations were identical during the first 5 ps, hence, R_{gyr} of both simulations coincide. However, when the electrostatic forces due to the solvent are switched on in *simulation B* the radii deviate. Nevertheless, R_{gyr} for both simulations fluctuate about the same equilibrium value and one can conclude that solvent effects due not unfold or compress BPTI.

Even if BPTI does not increase in size, its surface due to solvent interactions may still change through corrugation. The time dependence of the accessible surface of BPTI for *simulations A, B* is shown in Figure 7. One would expect that the solvent accessible surface increases through interactions with a solvent, the reason being that these interactions favour atoms with partial charges at the surface. In fact, one observes an increase of the solvent accessible surface after the common period of 5 ps in which both simulations are identical. However, the solvent-induced increase measures only about 70 Å^2, i.e., only about 2 percent of the total surface of BPTI. To judge this increase we note that the solvent accessible surface of a tyrosine side group is about 200 Å^2. This implies that the solvent, during the brief period of 15 ps, has only a minor affect on the corrugation of the surface of BPTI, inducing about a third of an amino acid side group the size of tyrosine to expose itself to the solvent. A more realistic description of the influence of the solvent which takes into account the slow relaxation behaviour of water as described in Section 2.4 is not likely to lead to larger changes of the shape of BPTI. An important improvement of the simulation of solvent effects may be obtained through an all-atom representation of water near the surface of the protein combined with a continuum water model in the peripheral region.

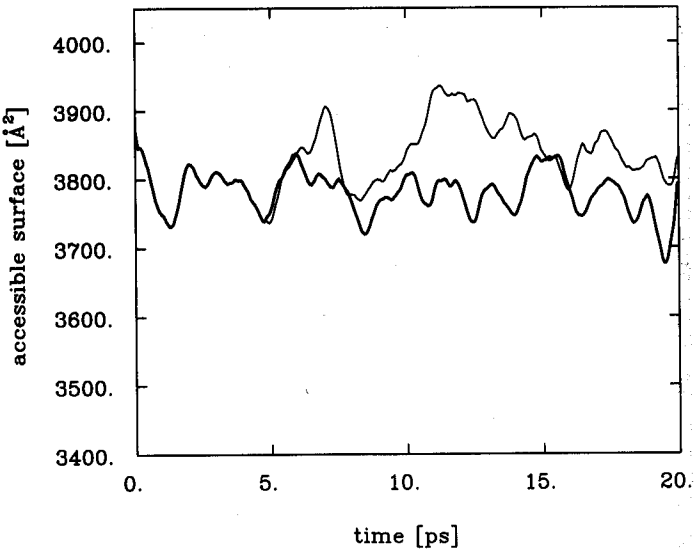

Figure 7 Time development of total solvent accessible surface of BPTI for molecular dynamics simulations A and B. The definition of solvent accessible surface is given in Section 2.1. The thick line refers to simulation A (protein in vacuum, full range electrostatic interactions are taken into account, parameters see Section 3.1), the thin line refers to simulation B (protein in solution, parameters for simulation and discretisation see Section 3.2 and 2.2.4). Both simulations started with the same protein structure (see definition of simulations A and B in Section 3.1 and 3.2). In simulation B, screening was switched on instantaneously at $t = 5$ ps.

3.3 *Effect of Surface Counter Charges*

A protein can interact with its environment also through charged chemical constituents, either through ions which bind to the surface, e.g., metal ions, or through protons which protonate or deprotonate surface-accessible amino acid side groups. Because of the immediate contact of such counter charges which can neutralize otherwise charged amino acid side groups, a stronger effect than that of a solvent can be expected. The placement of counter charges depends on one side on the pK-values of amino acids, on the other side on the affinities for ions. Both properties cannot be characterized easily theoretically. To investigate the effect of counter ions we choose, therefore, to place test charges through an energy optimization criterium on the surface of BPTI and to monitor the resulting dynamics. The results should not be interpreted as describing BPTI realistically, but rather to indicate in principle which effects ion binding and pK effects exert on a protein's structure.

BPTI carries a net charge of +6. We have chosen, therefore, six negative counter-charges at *hot spots* (see Section 2.3) to neutralize the protein. The simulation started from the equilibrated structure of BPTI which had been obtained as described in Section 2.4. We monitored during the corresponding *simulation C* the radius of gyration R_{gyr} as well as the surface accessible surface.

The time development of R_{gyr} and of the solvent accessible surface for a system with (*simulation C*) and without (*simulation A*) counter ions are presented in Figure 8 and Figure 9, respectively. Both properties are observed to decrease through interactions

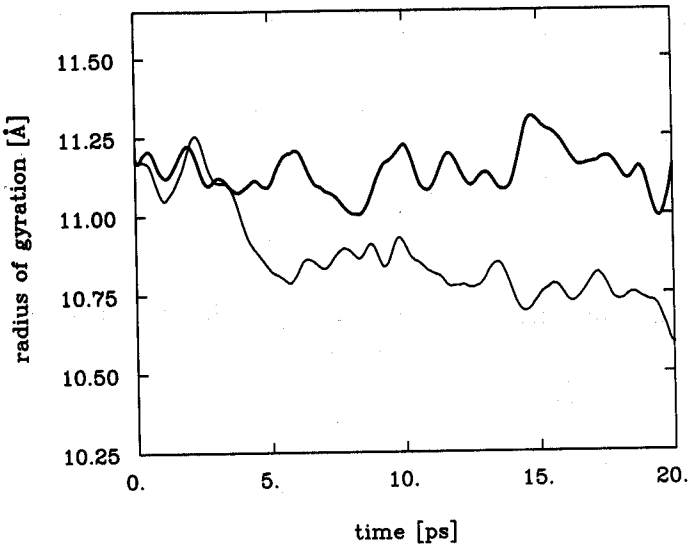

Figure 8 Time development of the radius of gyration of BPTI for molecular dynamics simulations A and C. The thick line corresponds to simulation A (protein in vacuum, see Section 3.1). The thin line corresponds to simulation C (protein interacts with 6 negative counter charges, see Section 3.3). In the case of simulation A, the protein has a net charge of +6, whereas in the case of simulation C, the protein-counter charge system is neutral. Both simulations started from the same protein structure. (see Section 2.4)

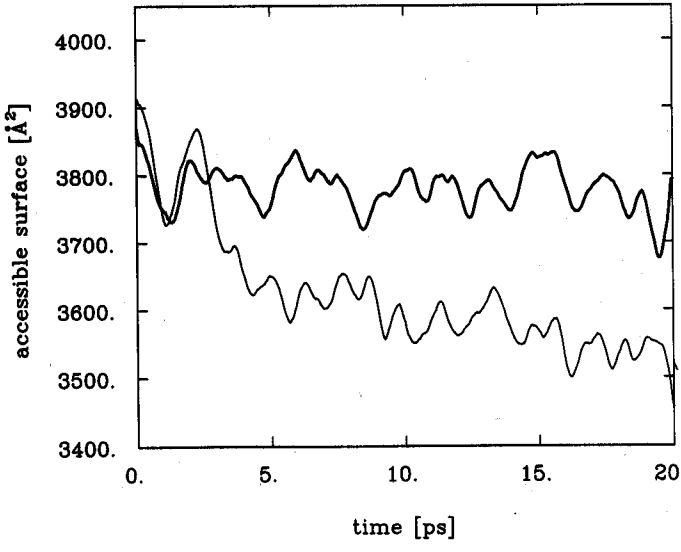

Figure 9 Time development of total solvent accessible surface of BPTI for molecular dynamics simulations A and C. The thick line corresponds to simulation A (protein in vacuum, see Section 3.1). The thin line corresponds to simulation C (protein interacts with 6 negative counter charges, see Section 3.3). In the case of simulation A, the protein has a net charge of +6, whereas in the case of simulation C, the protein-counter charge system is neutral. Both simulations started from the same protein structure. (see Section 2.4)

with counter charges. The radius of gyration decreases by about 0.5 Å during the simulation, the solvent accessible surface decreases by about 200 Å^2, which corresponds to the surface of one tyrosine side group (see Section 3.2) being transferred from the solvent to the interior of the protein. The results in Figure 8 and Figure 9 indicate that BPTI shrinks considerably in size through neutralization of its charged amino acids. One can conclude that the charge states of amino acids at the surface of a protein need to be considered carefully in simulations, e.g., by determining the pK_A values [23].

3.4 *Effect of a Finite Cut-off of Coulomb Forces*

We like to consider finally the effect of an approximation often employed for molecular dynamics, namely the cut-off of Coulomb forces beyond a certain distance [27]. Such approximation reduces the computational effort to determine pair interactions, the computationally most demanding step in molecular dynamics simulations of large polymers. The effect of this approximation can be understood well in the context of our present discussion since a cut-off of Coulomb forces implies that charged surface groups beyond the cut-off radius do not interact. One would expect that the cut-off has an effect similar to that of counter charges in that the size of electrostatic interactions between charged amino acid groups at the surface of the protein is reduced in both cases. To estimate the effect of using a finite cut-off radius compared to the effect of solvent screening as described by our model, we performed a simulation referred to as *simulation D* in which we assumed a cut-off radius of 10.5 Å. This simulation was started with the same protein configuration as *simulations A* and *B* (see Section 3 and Appendix B). We consider again the time development of the radius of gyration as well as the time development of the solvent accessible surface.

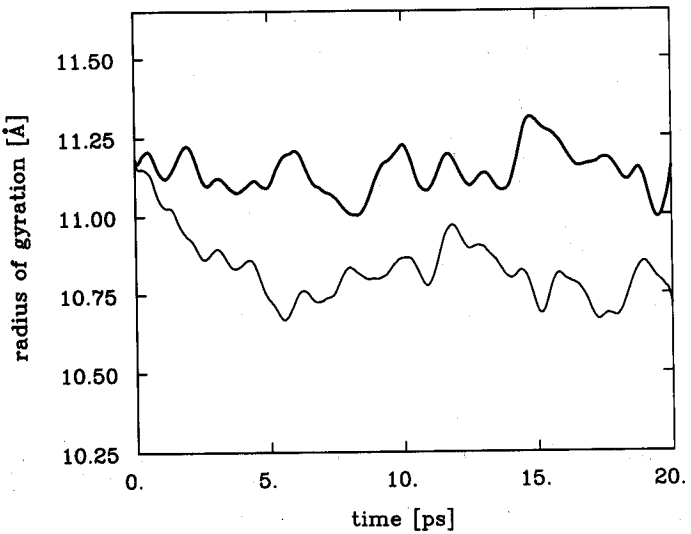

Figure 10 Time development of the radius of gyration of BPTI for molecular dynamics simulations A and D. The thick line corresponds to simulation A (protein in vacuum, all electrostatic interactions within the protein are taken into account as described in Section 3.1). The thin line corresponds to simulation D (protein in vacuum, only electrostatic interactions between atoms less than 10.5 Å apart are taken into account, see Section 3.4). Both simulations started from the same protein structure. (see Section 2.4)

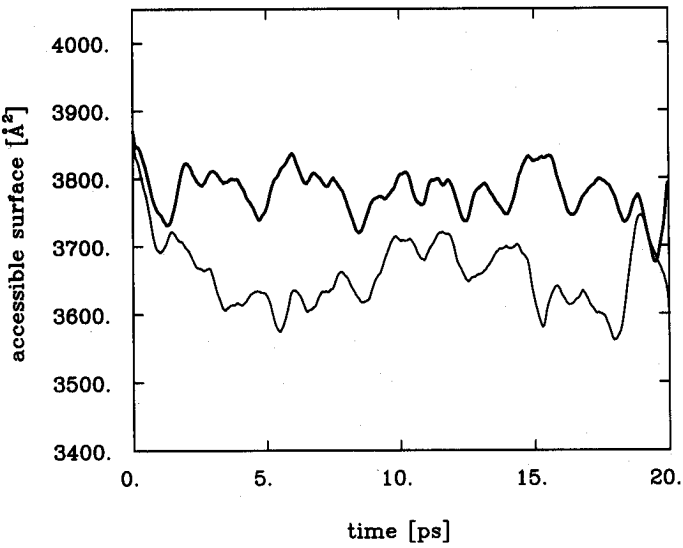

Figure 11 Time development of the solvent accessible surface of BPTI for molecular dynamics simulations A and D. The thick line corresponds to simulation A (protein in vacuum, all electrostatic interactions within the protein are taken into account as described in Section 3.1). The thin line corresponds to simulation D (protein in vaccum, only electrostatic interactions between atoms less than 10.5 Å apart are taken into account, see Section 3.4). Both simulations started from the same protein structure. (see Section 2.4)

results confirm the expectation that BPTI with a net positive charge experiences less intramolecular repulsion in the case of a cut-off of Coulomb forces and, as a result, decreases in size by about 0.5 Å in the radius of gyration. The decrease is due to the fact that some of the positive charges at the surface of BPTI are further apart than 10.5 Å and do not repel each other in *simulation D*. An analogous effect is found for the solvent accessible surface of BPTI which is presented in Figure 11. In case of *simulation D* the solvent accessible surface decreases by about 120 Å relative to that determined for *simulation A*. The decrease implies that a side group about half the size of tyrosine becomes burried when the Coulomb forces are cut off. These results suggest that molecular dynamics simulations which do not take electrostatic interactions faithfully into account can predict wrong shapes of biopolymers.

4 DISCUSSION

We have demonstrated that molecular dynamics simulations which account for solvent effects due to dielectric inhomogenities and Debye–Hückel screening are computationally feasible. We have discussed various computational approaches to represent screening potentials and the corresponding forces. Application to BPTI has revealed that in the case of this protein solvent effects, as judged by changes of radius of gyration and accessible surface area, are small. Yet we have found that counter charges which represent protonation/deprotonation processes or binding of ions, have a considerable effect on the shape of a protein, judged by the same criteria. Since

water and solvated ions in water can have a profound influence on pK_A's of surface groups and ion binding we expect that proper descriptions of proteins require a careful determination of pK_A values to determine the right protonation state of amino acids, for which purpose solvent effects need to be considered, and requires the inclusion of possible ion binding and solvent effects to account for a proper protein size and surface corrugation.

Presently, many efforts are being undertaken to improve technological approaches towards large scale protein molecular dynamics and protein electrostatics calculations [53, 21, 54]. The algorithms available today allow one to combine molecular dyamics studies with more faithful descriptions of solvent environments, either by explicitly simulating water around proteins [55], by involving continuum solvent models or a combination of both. Computation times for large proteins, e.g., about 70 ps for a protein of 12 000 atoms on a Cray 2 single processor using the program CHARMM, are about the same as needed for solving potential and force fields from integration of the Poisson–Boltzmann equation. If one employs parallel computers the computational tasks can be shared between processors and including proper solvent dielectric and Debye–Hückel effects should not degrade computational performance if one adds programs for molecular dynamics and for electrostatics.

We expect that future molecular dynamics studies will include solvent effects in a manner suggested here, most likely, however, in a combined molecular and continuum approach for the solvent. For many important outstanding problems in molecular dynamics, in particular, protein folding and protein modelling, improved descriptions of biopolymer (proteins, DNA, RNA, etc.) – solvent interactions are critical and algorithmic and conceptual developments for better descriptions of this interactions will determine further progress.

References

[1] C. Niedermeier, "Elektrostatische Kontrolle der Primärprozesse im phytosynthesischen Reaktionszentrum von Rhodopseudomonas viridis", Master's thesis, Technische Universität München, München, January 1989.

[2] W. Kauzmann, *Adv. protein Chem.*, **14,** 1 (1959).

[3] C. Tanford, " The Hydrophobic Effect". John Wiley & Sons, Inc., New York, 1980.

[4] T.E. Creighton, "Proteins". W.H. Freeman and Company, San Francisco, 1984.

[5] L. Stryer, "Biochemistry". W.H. Freeman and Company, San Francisco, 1988.

[6] A. Warshel, "Energetics of enzyme catalysis", *Proc. Natl. Acad. Sci. USA*, **75,** 5250 (1978).

[7] I. Klapper, R. Hagstrom, R. Fine, K. Sharp, and B. Honig, "Focussing of electric fields in the active site of cu-zn superoxide dismutase: Effects of ionic strength and amino-acid modification", *Proteins*, **1,** 47 (1986).

[8] A. Warshel, G. Naray-Szabo, F. Sussman, and J.-K. Hwang, "How do serine proteases really work?", *Biochemistry*, **28,** 3629 (1989).

[9] A.T. Hagler and J. Moult, "Computer simulation of the solvent structure around biological macromolecules", *Nature.*, **272,** 222 (1978).

[10] J. Hermans, H.J. Berendsen, W.F. van Gunsteren, and J.P. Postma, "A consistent empirical potential for water-protein interactions", *Biopolymers*, **23,** 1513 (1984).

[11] P.J. Rossky and M. Karplus, "Solvation. A molecular dynamics study of a dipeptide in water", *J. Am. Chem. Soc.*, **101,** 1913 (1979).

[12] S.T. Russel and A. Warshel, "Calculations of electrostatic energies in proteins: The energetics of ionized groups in bovine pancreatic trypsin inhibitor", *J. Molec. Biol.*, **185,** 389 (1985).

[13] J. Warwicker and H.C. Watson, "Calculation of the electric potential in the active site cleft due to α-helix dipoles", *J. Molec. Biol.*, **157,** 671 (1982).

[14] M.J.E. Sternberg, F.R.F. Hayes, A.J. Russell, P.J. Thomas, and A.R. Fersht, "Prediction of electrostatic effects of engineering of protein charges", *Nature.*, **303,** 86 (1987).

[15] R.J. Zauhar and R.S. Morgan, "A new method for computing the macromolecular electric potential", *J. Molec. Biol.*, **186,** 815 (1985).
[16] J.A. McCammon, B.R. Gelin, and M. Karplus, "Dynamics of folded proteins", *Nature.*, **267,** 585 (1977).
[17] W.F. van Gunsteren and H.J.C. Berendsen, "Algorithms for macromolecular dynamics and constraint dynamics", *Molec. Phys.*, **34,** 1311 (1977).
[18] M. Levitt, "Molecular dynamics of native proteins. ii. Analysis and nature of motion", *J. Molec. Biol.*, **168,** 621 (1983).
[19] W.F. van Gunsteren and M. Karplus, "Protein dynamics in solution and in a crystalline environment: A molecular dynamics study", *Biochemistry,* **21,** 2259 (1982).
[20] A. Warshel, F. Sussman, and G. King, "Free energy of charges in solvated proteins: Microscopic calculations using a reversible charging process", *Biochemistry,* **25,** 8368 (1986).
[21] M.K. Gilson and B.H. Honig, "Calculation of the total electrostatic energy of a macromolecular system: Solvation energies, binding energies and conformational analysis", *Proteins,* **47,** (1988).
[22] D. Eisenberg and A.D. McLachlan, "Solvation energy in protein folding and binding", *Nature.*, **319,** 198 (1986).
[23] A. Warshel, "Calculations of chemical processes in solution", *J. Phys. Chem.*, **83,** 1640 (1979).
[24] H.L. Friedmann, *Molec. Phys.*, **29,** 1533 (1975).
[25] R.O. Watts, *Chem. Phys.*, **57,** 185 (1981).
[26] J.D. Jackson, "Classical Electrodynamics". John Wiley & Sons, Inc., New York, 1975.
[27] B.R. Brooks, R.E. Bruccoleri, B.D. Olafson, D.J. States, S. Swaminathan, and M. Karplus, 'Charmm: A program for macromolecular energy minimization, and dynamics calculations", *J. Comp. Chem.*, **4,** 187 (1983).
[28] J.A. McCammon and S.C. Harvey, "Dynamics of Proteins and Nucleic Acids". Cambridge University Press, Cambridge, 1987.
[29] M. Berkowitz and J.A. McCammon, "Molecular dynamics with stochastic boundary conditions", *Chem Phys. Lett.*, **90,** 215 (1982).
[30] C.L. Brooks, A. Brünger, and M. Karplus, "Active site dynamics in protein molecules: A stochastic boundary molecular-dynamics approach", *Biopolymers,* **24,** 843 (1985).
[31] B. Lee and F.M. Richards, "The interpretation of protein structure: Estimation of static accessibility", *J. Molec. Biol.*, **55,** 379 (1971).
[32] S.C. Harvey, "Treatment of electrostatic effects in macromolecular modeling", *Proteins,* **5,** 78 (1989).
[33] J.G. Kirkwood, "Theory of solution of molecules containing widely separated charges with special applications for zwitterions", *J. Chem. Phys.*, **2,** 351 (1934).
[34] C. Tanford and J.G. Kirkwood, "Theory of protein titration curves", *J. Am. Chem. Soc.*, **79,** 5333 (1957).
[35] M.K. Gilson and B.H. Honig, "Calculation of electrostatic potentials in an enzyme active site", *Nature,* **330,** 84 (1987).
[36] M.K. Gilson, K.A. Sharp, and B.H. Honig, "Calculating the electrostatic potential of molecules in solution: Method and error assessment", *J. Comp. Chem.*, **9,** 327 (1987).
[37] W.H. Press, B.P. Flannery, S.A. Teukolsky, and W.T. Vetterling, "Numerical Recipes in C". Cambridge University Press, Cambridge, 1988.
[38] A. Brandt, "Guide to multigrid development", in: W. Hackbusch and U. Trottenberg, eds, "Multi-Grid Methods", page 220, Berlin, Heidelberg, New York, 1982. Springer-Verlag.
[39] A. Brandt, "Algebraic multigrid theory: The symmetric case.", in: "Preliminary Proc. Int. Multigrid Conf.", Copper Mountain, Colorado, 1983.
[40] W. Hackbusch, "Multi-Grid Methods and Applications". Springer-Verlag, Berlin, Heidelberg, New York, 1985.
[41] M.L. Connolly, "Solvent-accessible surfaces of proteins and nucleic acids", *Science,* 5730 (1987).
[42] U. Singh, S. Weiner, and P. Kollman, "Molecular dynamics simulations of d(cgcga)·(tcgcg) with and without hydrated counterions", *Proc. Natl. Acad. Sci. USA,* **82,** 755 (1985).
[43] B. Tidor, K. Irikura, B. Brooks, and M. Karplus, "Dynamics of DNA oligomers", *J. Biol. Strut. Dyn.*, **1,** 231 (1983).
[44] M. Karplus and J.A. McCammon, "Dynamics of proteins: Elements and function", *Ann. Rev. Biochem.*, **53,** 263 (1983).
[45] M. Karplus and D.L. Weaver, "Protein folding dynamics", *Nature,* **260,** 404 (1976).
[46] R. Elber and M. Karplus, "Multiple conformational states of proteins: A molecular dynamics analysis of myoglobin", *Science,* **235,** 318 (1987).
[47] R.M. Levy, R.P. Sheridan, J.W. Keepers, G.S. Dubey, S. Swaminathan, and M. Karplus, "Molecular dynamics of myoglobin at 298°K: Results from a 300-ps computer simulation", *Biophys. J.*, **48,** 509 (1985).

[48] W. Nadler, A.T. Brünger, K. Schulten, and M. Karplus, "Molecular and stochastic dynamics of proteins", *Proc. Natl. Acad. Sci. USA*, **84**, 7933 (1987).
[49] M. Karplus and J.A. McCammon, "The dynamics of proteins", *Scient. Am.*, **4**, 30 (1986).
[50] W.F. van Gunsteren, "Computer simulation by molecular dynamics as a tool for modelling of molecular systems", *Molec. Sim.*, **3**, 187 (1989).
[51] A.T. Brünger, "Crystallographic refinement by simulated annealing", in: N.W. Isaacs and M.R. Taylor, eds, "Crystallographic computing 4: Techniques and new technologies", Oxford, 1988. Clarendon Press.
[52] J. Deisenhofer and W. Steigemann, "Crystallographic refinement of the structure of bovine pancreatic trypsin inhibitor at 1.5 Å resolution", *Acta Cryst. B*, **31**, 238 (1975).
[53] A. Warshel and S.T. Russel, "Calculations of electrostatic interactions in biological systems and in solution", *Q. Rev. Biophys.*, **17**, 283 (1984).
[54] J.J. Wendoloski and J.B. Matthew, "Molecular dynamics effects on protein electrostatics", *Proteins*, **5**, 313 (1989).
[55] M. Levitt and R. Sharon, "Accurate simulation of protein dynamics in solution", *Proc. Natl. Acad. Sci. USA*, **85**, 7557 (1988).

APPENDIX A ANALYTICAL SOLUTION

The linearized Poisson–Boltzmann Equation (4) can be solved analytically for problems with spherical geometry. Unlike Tanford and Kirkwood [34], we will give a general solution for arbitrary charge distributions, i.e., also for continuous charge distributions, in the form of a Greens function. The Greens function obtained can be used to represent atomic charges by spherical charge clouds rather than by point charges, which is a more accurate way to represent the charge distribution of a molecule.

We consider a spherical region of radius R with dielectric constant ε, and vanishing Debye–Hückel parameter which is surrounded by a medium with dielectric constant ε_ρ and a Debye–Hückel parameter κ. For this problem, the linearized Poisson–Boltzmann equation reads

$$\Delta\Phi(\mathbf{r}) = -\frac{4\pi}{\varepsilon_s}\rho(\mathbf{r}) \qquad \text{if } r < R \tag{30}$$

$$(\Delta - \bar{\kappa}^2)\Phi(\mathbf{r}) = -\frac{4\pi}{\varepsilon_r}\rho(\mathbf{r}) \qquad \text{if } r > R$$

where $\bar{\kappa} = \kappa/\sqrt{\varepsilon_r}$. The Greens function for this problem is obtained by solving the differential equations which result from (30) when $\rho(\mathbf{r})$ is substituted by the delta function $\delta(\mathbf{r}-\mathbf{r}')$. One obtains (for details see [1])

$$G_s(\mathbf{r},\mathbf{r}') = \frac{4\pi}{\varepsilon_s}\sum_{l=0}^{\infty}\sum_{m=-l}^{l}\frac{Y^*_{lm}(\theta',\phi')\,Y_{lm}(\theta,\phi)}{2l+1}\,r_<^{l+1}\left(\frac{1}{r_>^{l+1}} - \frac{r_>^l}{R^{2l+1}}\right) \tag{31}$$

in the spherical region ($r < R$) and

$$G_p(\mathbf{r},\mathbf{r}') = \frac{-4\pi i\bar{\kappa}}{\varepsilon_p}\sum_{l=0}^{\infty}\sum_{m=-l}^{l}Y^*_{lm}(\theta',\phi')Y_{lm}(\theta,\phi)\,\frac{h_l^{(1)}(i\bar{\kappa}r)}{h_l^{(1)}(i\bar{\kappa}R)}$$

$$\times\,[j_l(i\bar{\kappa}r_<)n_l(i\bar{\kappa}R) - n_l(i\bar{\kappa}r_<)j_l(i\bar{\kappa}R)] \tag{32}$$

in the peripheral region ($r > R$). $r_>$ ($r_<$) is the larger (smaller) of $|\mathbf{r}|$ and $|\mathbf{r}'|$, the $Y_{lm}(\theta,\phi)$ are spherical harmonics and $j_l(x)$, $n_l(x)$ and $h_l^{(1)}(x)$ denote the spherical Bessel, Neumann and Hankel functions of order l, respectively.

The Greens function obtained can be applied to solve the spherical problem for an arbitrary charge distribution $\rho(\mathbf{r})$. By evaluating

$$\Phi(\mathbf{r}) = \int_V \rho(\mathbf{r}) G(\mathbf{r},\mathbf{r}') d^3 r - \frac{1}{4\pi} \oint_S \Phi(\mathbf{r}') \frac{\partial G(\mathbf{r},\mathbf{r}')}{\partial n'} 45 da da' \tag{33}$$

solutions for the spherical and the peripheral region can be obtained. The potential on the surface S of the spherical region $|\mathbf{r}| < R$, which has to be known to evaluate the surface integral in (33), is formally expanded in terms of spherical harmonics, namely

$$\Phi(\mathbf{r}') \Big|_{r'=R} = \sum_{l=0}^{\infty} \sum_{m=-l}^{l} A_{lm} Y_{lm}(\theta',\phi'). \tag{34}$$

The coefficients A_{lm} are determined (see [1]) by exploiting the continuity of $D_\perp$ at the dielectric interface yielding the condition

$$\varepsilon_s \frac{\partial \Phi_s}{\partial r}\Big|_{r=R} = \varepsilon_p \frac{\partial \Phi_p}{\partial r}\Big|_{r=R}, \tag{35}$$

where Φ_s and Φ_p are the solutions in the spherical and the peripheral region, respectively.

For a charge distribution of N point charges q_j at positions $\mathbf{r}_j$ within the spherical region and vanishing charge density in the peripheral region one obtains the solution given by Kirkwood [33]

$$\Phi_s(\mathbf{r}) = \sum_{l=0}^{\infty} \sum_{m=-l}^{l} \left\{ \sum_{j=1}^{N} K_{lmj}(r,r_j) + \frac{(2l+1)\varepsilon_s}{\eta_l \varepsilon_p + l\varepsilon_s} M_{lm} \left(\frac{r}{R}\right)^l \right\} Y_{lm}(\theta,\phi) \tag{36}$$

$$\Phi_p(\mathbf{r}) = \sum_{l=0}^{\infty} \sum_{m=-l}^{l} \frac{(2l+1)\varepsilon_s}{\eta_l \varepsilon_p + l\varepsilon_s} M_{lm} \frac{h_l^{(1)}(i\bar{\kappa}r)}{h_l^{(1)}(i\bar{\kappa}R)} Y_{lm}(\theta,\phi) \tag{37}$$

where

$$\eta_l = -i\bar{\kappa}R \frac{h_l^{(1)\prime}(i\bar{\kappa}R)}{h_l^{(1)}(i\bar{\kappa}R)} \tag{38}$$

and

$$K_{lmj}(r,r_j) = \frac{4\pi}{2l+1} \frac{q_j}{\varepsilon_s} r_<^l \left(\frac{1}{r_>^{l+1}} - \frac{r_>^l}{R^{2l+1}} \right) Y_{lm}^*(\theta_j,\phi_j), \tag{39}$$

$$M_{lm} = \frac{4\pi}{2l+1} \sum_{j=1}^{N} \frac{q_j}{\varepsilon_s R} \left(\frac{r_j}{R}\right)^l Y_{lm}^*(\theta_j, \phi_j). \tag{40}$$

In Equation (39) $r_>$ ($r_<$) denotes again the larger (smaller) of r and r_j.

APPENDIX B PARAMETER FOR THE SIMULATIONS

The following simulation parameters were used in *simulations A, B, C* and *D*:

Property	*Sim. A*	*Sim. B*	*Sim. C*	*Sim. D*
total charge [e_0]	+6	+6	0	+6
cut-off radius [Å]	∞	∞	∞	10.5
time step of integration [fs]	1	1	1	1
dielectric constant of protein	2	2	2	2
dielectric constant of water	–	80	–	–
Debye–Hückel parameter [$Å^{-1}$]	–	.125	–	–

The inclusion of solvent screening in simulation B is described in Section 2.4. In this simulation, the dielectric constant $\varepsilon_w = 80$ and the Debye–Hückel parameter $\kappa = 0.125\,Å^{-1}$ for water were chosen. The linearized Poisson–Boltzmann equation was solved using the finite difference algorithm as described in Section 2.2.2. The finest resolution of the discretization lattice was 1 Å in the protein region, and 4 Å in the boundary region (see Section 2.2.4). The size of the solute volume in which the electrostatic potential was determined is $64 \times 64 \times 64\,Å^3$. The screening potential $\delta\Phi$ was updated every 250 fs. In *simulation B*, the atomic velocities were rescaled throughout the whole simulation to keep the temperature stable.